




**Anisotropic electron transport Rashba effects in valleytronics**V. A. Kochelap  and V. N. Sokolov <sup>\*</sup>*Department of Theoretical Physics, Institute of Semiconductor Physics,  
National Academy of Sciences of Ukraine, Pr. Nauki 41, Kiev 03028, Ukraine* (Received 13 October 2022; revised 21 November 2022; accepted 22 November 2022; published 20 December 2022)

Electrically induced space separation of free carriers of different valleys in bulk multivalley semiconductors with restricted geometry was first reported by Rashba in 1965. This Rashba's size effect remains relevant at the present time for the rapidly developing field of valleytronics. In this paper, we investigate theoretically electrically induced formation of valley-polarized free-carrier domains in two-dimensional (2D) many-valley semiconductor nanosystems with equivalent anisotropic valleys such as in *n*-Si, *n*-AlAs, etc. The domains are well-resolved spatial regions in which the electrons of only one of the valleys are present, thereby providing a pure bulk valley current inside the considered domain region. The domain properties including the polarization amplitude, the domain wall width, configurations of the induced transverse electric fields, valley currents, and the excess electric charge density are analyzed as a function of the applied electric field *E*. The valley-polarized domains in the nanostrip generate inhomogeneous electrostatic potential outside the strip and give rise to stratification of the induced by the current magnetic field consistent with the valley-polarized domains. These effects facilitate experimental verification of the valley polarization by the existing methods of scanning nanoscale imaging. We suggest that the study of electrically induced domains of valley polarization in 2D nanosystems brings new knowledge on valley physics and can be used in valleytronics applications.

DOI: [10.1103/PhysRevB.106.245422](https://doi.org/10.1103/PhysRevB.106.245422)**I. INTRODUCTION**

This paper acknowledges the outstanding physicist E. I. Rashba whose contribution to the solid state physics is great and diverse. Thus, widely known are his bright works on the symmetry of crystals, spin-orbit, and electron-phonon interactions in semiconductors, as well as on excitons. Among his numerous works [1], an important place is also occupied by studies of the phenomena of the carrier transport in semiconductors, which were carried out during his earlier years (1965–1976) [2–10]. In the cycle of these works, he paid attention to the features of energy band structure and, in particular, to the behavior of various groups of the free carriers such as electrons and holes, the electrons of different valleys, etc. It is important to note that the research on multivalley semiconductors initiated by Rashba remains relevant to the present time. Thus, for example, space separation of the electrons of different valleys in multivalley semiconductors restricted by the transverse dimension (relative to the direction of the applied electric field), i.e., the Rashba size effect [2], is exhibited in the modern quantum nanostructures [11], which potentially present perspective element base for the emerging new field of nanoelectronics: valleytronics.

In recent years, the field of valleytronics [12] (valley-dependent electronics [13] and optoelectronics [14]) has emerged, motivated by the potential of using the valley degree of freedom for information processing and storage applications, similar to spin in spintronics [15]. The major aspects of

valleytronics concern the generation, manipulation, and detection of valley-polarized charge carriers and electric currents. Such ability for valley polarization has been demonstrated in experiments with various multivalley systems: traditional bulk semiconductors such as germanium [16], diamond [17], and bismuth [18], as well as modern two-dimensional (2D) nanostructures; for example, AlAs quantum wells (QWs) [19–21], ultrahigh mobility Si(111) nanostructures [22–26], 2D honeycomb lattice systems lacking spatial inversion symmetry such as graphene nanostructures [27,28], and group-VI transition metal dichalcogenides (TMDs) [29–34], etc. Also, the importance of the valley degeneracy has been shown for 2D transport properties in Si(111)-vacuum field-effect transistors (FETs) and Si-based metal-oxide-semiconductor FET configurations [35].

The valley-dependent electric properties of semiconductors with multiple valleys in the conduction and/or valence bands have been in the focus of investigations in the past few decades. Examples highlighting the achievements in fundamental valley physics and device applications including early works can be mentioned for different states of the carriers: thermodynamically equilibrium carriers (multivalley Jahn-Teller-type effect) [36–40]; nonequilibrium carriers under nonheating electric fields (anisotropic size effects) [3,10], heating fields for crystals with equivalent valleys (many-valued Sasaki-Shibuya effect) [41,42], and nonequivalent valleys (the Gunn effect) [43].

It is noted that among different ways of generating the valley polarization (electrical [16,17,33,34], optical [30], under an external magnetic field [18], or strain [44–46]) the pure electrical method is most preferable for potential applications

<sup>\*</sup>sokolov@isp.kiev.ua

[13]. One possible way for *all-electrical* manipulation of the valley degree of freedom is based on the use of electrical anisotropy of different valleys inherent in the valley energy spectrum. In this case, generally, the valley electric current is directed at an angle to the vector of the applied electric field. For the formation of valley-polarized domains which are of interest here, we focus on the following two examples of anisotropic valleys for which crystallographic orientation and carrier population can be effectively controlled.

(i) *2D electrons in AlAs QWs*. The electrons occupy conduction-band valleys at the  $X$  points of the Brillouin zone. It is noted that in QWs of large well's thicknesses with the growth direction along [001] ( $z$  direction), only the lowest in-plane  $x$  and  $y$  valleys are occupied, thus rendering a simple *two-valley* system [21].

(ii) *2D electrons on Si(111) surfaces*. In bulk Si, six equivalent conduction-band valleys are located along [100]-type directions in the momentum  $\mathbf{k}$  space, where two valleys in the same axis are treated as one valley. It has been shown that the H-Si(111)/vacuum interface gated through a vacuum barrier provides a high electron mobility with sixfold valley degeneracy [22–25,35], thus rendering the more complex *three-valley* system.

A feature of the domains under consideration is that they arise during the passage of electric current in a transversely bounded sample, where the current generates nonequilibrium electrons of different valleys in the regions at the side edges, and the gradients of the electron concentrations and the induced electric field are directed across the direction of the current. In considering the projection of six constant energy ellipsoids in the Brillouin zone from the bulk onto (111) plane, the valleys are projected equally with sixfold symmetry [22,23]. For the analysis simplicity, we consider symmetrical orientation of the valleys in relation to the nanostructure edges. In this case, there are two variants of the sample geometry where the side edges are parallel to  $[11\bar{2}]$  ( $\gamma = \pi/6$ ) or  $[\bar{1}10]$  ( $\gamma = \pi/3$ ) crystallographic axes (Fig. 1). We define  $\gamma$  as the angle between the  $y$  axis [i.e.,  $[\bar{1}10]$  ( $\gamma = \pi/6$ ) or  $[11\bar{2}]$  ( $\gamma = \pi/3$ )] and the long principal axis of the valley 2. Qualitatively, the situation is as follows. Under the electric field, two of the valleys create electron flows to the edges  $y = d \equiv d_y/2$  (valley 2) and  $y = -d$  (valley 1), while valley 3 is located in  $[11\bar{2}]$  axis which is one of its principal axes and, therefore, does not create electron flows to the edges. An arbitrary valley orientation can be incorporated within the same theoretical model.

The rest of the paper is organized as follows. In Sec. II, we describe the theoretical model and main equations used for the electron drift-diffusion transport in the 2D multivalley system with geometrical dimensions essentially restricted in the transverse direction relatively to the electric current. Using simple qualitative considerations, we demonstrate the possibility of the valley domains formation induced by the electric current in case of arbitrary number of valleys. In Sec. III, we develop the theory for valley-polarized domains in the absence of intervalley scattering of the 2D electrons. Section IV provides an extension of the theory to the case of arbitrary intervalley scattering rates. The discussion on the obtained results is given in Sec. V, which is followed by a brief summary in Sec. VI. In the Appendix, we describe the

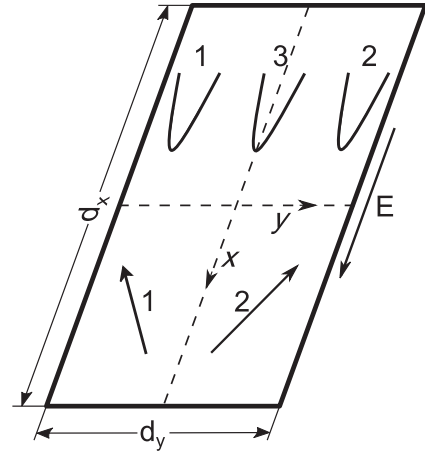


FIG. 1. Schematic illustration of the sample geometry of rectangular form ( $d_x \gg d_y$ ) made of a 2D Si(111) QW nanostructure for the electrically induced valley-polarization domains. The electric field  $E_x = E$  is applied along the  $x$  axis. The skewed arrows 1 and 2 depict the electron flows of the anisotropic valleys (1 and 2, respectively) to the sample edges parallel to  $[11\bar{2}]$  ( $\gamma = \pi/6$ ) or  $[\bar{1}10]$  ( $\gamma = \pi/3$ ).

details of analytical solution of the nonlinear drift-diffusion equations, the Poisson equation, and the induced magnetic field normal to the nanostructure plane.

## II. MODEL AND BASIC EQUATIONS

For the electron transport in the considered multivalley low-dimensional system, we assume the intervalley scattering rate ( $\sim \tau^{-1}$ ) to be much slower than the intravalley scattering rates of the electron momentum ( $\sim \tau_p^{-1}$ ) and energy ( $\sim \tau_\varepsilon^{-1}$ ). This implies certain inequalities on the characteristic scattering times  $\tau \gg (\tau_p, \tau_\varepsilon)$ . In this case, the transport behavior of the free carriers in each valley  $\alpha$  ( $\alpha = 1, \dots, \nu$ , where  $\nu$  is the total number of valleys) can be described independently by individual valley electron densities  $n_\alpha$  and tensors of the kinetic coefficients such as the carrier mobility  $\mu_{ij}^{(\alpha)}$ , diffusivity  $D_{ij}^{(\alpha)}$ , etc. For specific geometry of a 2D nanostructure ( $d_x \gg d_y$ , Fig. 1) with the length  $d_x$  in the  $x$  direction and the width  $d_y = 2d$  in the  $y$  direction, the following components of valley currents are involved:

$$j_x^{(\alpha)} = -\mu_{xx}^{(\alpha)} n_\alpha E_x - \mu_{xy}^{(\alpha)} n_\alpha E_y - D_{xy}^{(\alpha)} \frac{dn_\alpha}{dy}, \quad (1)$$

$$j_y^{(\alpha)} = -\mu_{yx}^{(\alpha)} n_\alpha E_x - \mu_{yy}^{(\alpha)} n_\alpha E_y - D_{yy}^{(\alpha)} \frac{dn_\alpha}{dy}. \quad (2)$$

Here,  $E_x = E (>0)$  is the applied electric field and  $E_y$  is the induced electric field arising in a transversely bounded sample with anisotropic valleys. The transverse electric field  $E_y$  is determined by the Poisson equation. However, to explore the quasineutral intervalley redistributions of the carriers, it is sufficient to invoke the quasineutrality condition

$$\sum_{\alpha=1}^{\nu} n_\alpha = \nu n_0 = N, \quad (3)$$

where  $N$  is the total carrier density. Then,  $E_y$  can be found from the equation

$$j_y = \sum_{\alpha=1}^{\nu} j_y^{(\alpha)} = 0, \quad (4)$$

which corresponds to the absence of electric current in the  $y$  direction (an open-circuit condition). Thus, we obtain

$$E_y = - \left[ E \sum_{\alpha=1}^{\nu} \mu_{yx}^{(\alpha)} n_{\alpha} + \sum_{\alpha=1}^{\nu} D_{yy}^{(\alpha)} \frac{dn_{\alpha}}{dy} \right] / \sum_{\alpha=1}^{\nu} \mu_{yy}^{(\alpha)} n_{\alpha}. \quad (5)$$

Substituting  $E_y$  given by Eq. (5) in Eq. (2) and using the continuity equations

$$\frac{dj_y^{(\alpha)}}{dy} = - \sum_{\beta \neq \alpha} \frac{n_{\alpha} - n_{\beta}}{\tau}, \quad (6)$$

we obtain a closed system of  $\nu$  equations for the electron densities  $n_{\alpha}(y)$  in different valleys. The boundary conditions (BCs) to these equations are chosen in the form

$$j_y^{(\alpha)}(y = \pm d) = \pm \sum_{\beta \neq \alpha} S_{\alpha\beta}^{\pm} (n_{\alpha}^{\pm} - n_{\beta}^{\pm}), \quad (7)$$

where the superscripts ( $\pm$ ) stand for the sample edges  $y = \pm d$ , and  $S_{\alpha\beta}^{\pm}$  are the rates of the edge intervalley scattering. We note that Eq. (4), corresponding to an open-circuit condition, conforms to Eqs. (6) and (7). Indeed, if we sum these equations over the valley index  $\alpha$ , we obtain  $dj_y(y)/dy = 0$ ; then  $j_y(y) = \text{const}$ , and  $j_y(y = \pm d) = 0$  which finally gives  $j_y(y) = 0$ . Evidently, the alternative option is  $j_y \neq 0$ . In this case, the BCs can depend on specific properties of the edges as well as the employed external circuit: e.g., the selectivity of electron currents of different valleys flowing through the interface, etc.

The possibility of valley domains formation can be seen by considering the theoretical limit of strong electric fields ( $E \rightarrow \infty$ ) when the intervalley scattering in the sample bulk becomes not essential. The carrier densities  $n_{\alpha}(y)$  can be found from Eq. (2) by dividing both sides by  $E$  and replacing  $j_y^{(\alpha)}/E$ , for large values of  $E$  and finite  $S_{\alpha\beta}^{\pm}$ , by zero. Then, we have

$$a_{\alpha} n_{\alpha} + b_{\alpha} n_{\alpha} \frac{E_y}{E} + \frac{1}{E} \frac{dn_{\alpha}}{dy} = 0, \quad (8)$$

where  $a_{\alpha} = \mu_{yx}^{(\alpha)}/D_{yy}^{(\alpha)}$  and  $b_{\alpha} = \mu_{yy}^{(\alpha)}/D_{yy}^{(\alpha)}$ . Substituting  $E_y$  [Eq. (5)] into Eq. (8), we obtain

$$n_{\alpha} \sum_{\beta=1}^{\nu} D_{yy}^{(\beta)} n_{\beta} \left[ a_{\alpha} b_{\beta} - a_{\beta} b_{\alpha} + \frac{1}{E} \frac{d}{dy} \ln \left( \frac{n_{\alpha}^{b_{\beta}}}{n_{\beta}^{b_{\alpha}}} \right) \right] = 0. \quad (9)$$

Further, neglecting the small last term ( $\propto E^{-1}$ ) in the square brackets and taking into account the quasineutrality condition (3), we find that Eq. (9) has the solutions  $n_{\beta} = N \delta_{\alpha\beta}$ , with  $E_y = -(a_{\alpha}/b_{\alpha})E$ , where  $\alpha = 1, 2, \dots, \nu$ . The omitted small term may become finite in narrow regions of the width  $\sim E^{-1}$  where the coordinate derivative can be large; such regions form transition layers (domain walls) between the adjacent domains occupied exclusively by the electrons of only one of the valleys.

The above qualitative considerations demonstrate clearly the valley domains formation induced by the electrical current flowing through the sample under the applied electric field  $E$ . The domains consecutive order along the  $y$  coordinate is determined by the specific many-valley band structure as well as the imposed BCs at the nanostructure edges  $y = \pm d$ .

### III. TWO-DIMENSIONAL ELECTRONS AT A Si(111) SURFACE

In this section, we analyze the formation of valley-polarized domains under a weak intervalley scattering which is assumed for both the sample bulk and the edges. This model allows us to solve the nonlinear drift-diffusion equations exactly in analytical form.

We consider three conduction-band valleys corresponding to a Si(111) surface [22] for the nanostructure with geometry characteristics described in the previous section and depicted in Fig. 1. The system of coupled equations for the carrier densities  $n_{\alpha}$  in different valleys ( $\alpha = 1, 2, 3$ ) follows from Eqs. (6) and (7). In the limit of infinitely long intervalley scattering time ( $\tau \rightarrow \infty$ ), the equations can be written as

$$\begin{aligned} \frac{dn_1}{dy} &= -a_1 E_x n_1 - b_1 E_y n_1, \\ \frac{dn_2}{dy} &= a_1 E_x n_2 - b_1 E_y n_2, \\ \frac{dn_3}{dy} &= -b_3 E_y n_3, \end{aligned} \quad (10)$$

supplemented with the quasineutrality condition of Eq. (3):

$$n_1 + n_2 + n_3 = N. \quad (11)$$

Here, the symmetry properties of the valley electron mobilities  $\mu_{xy}^{(1)} = -\mu_{xy}^{(2)}$ ,  $\mu_{yy}^{(1)} = \mu_{yy}^{(2)}$ , and the diffusion coefficients  $D_{yy}^{(1)} = D_{yy}^{(2)}$  have been taken into account. As only two of the three valleys generate transverse electron flows to the edges (Fig. 1), it is convenient to use the variables associated with these valleys  $n_+ = n_1 + n_2$ ,  $n_- = n_1 - n_2$ . We add and subtract the first two equations in (10) to obtain

$$\begin{aligned} \frac{dn_+}{dy} &= -a_1 E_x n_- - b_1 E_y n_+, \\ \frac{dn_-}{dy} &= -a_1 E_x n_+ - b_1 E_y n_-, \end{aligned} \quad (12)$$

where  $E_y$  is expressed as

$$E_y = - \frac{a_1 n_-}{(b_1 - b_3) n_+ + b_3 N} E_x. \quad (13)$$

The solution of Eqs. (12) and (13) allows one to calculate transverse distributions of the valley carrier densities  $n_1 = (n_+ + n_-)/2$ ,  $n_2 = (n_+ - n_-)/2$ , and  $n_3 = N - n_+$ , as well as the induced electric field  $E_y$  for different values of the applied electric field  $E_x$ .

Further, for simplicity, the analysis is evolved assuming nondegenerate statistics to avoid additional nonlinearities inherent in the degenerate carriers. This assumption facilitates to solve the nonlinear differential equations (12) and (13) analytically. Using the Einstein relations  $\mu_{ij}^{(\alpha)} =$

$(e_0/k_B T)D_{ij}^{(\alpha)}$ , the parameters below Eq. (8) are expressed as  $a_1 = ae_0/k_B T$ ,  $b_1 = b_3 = e_0/k_B T$ , where  $a = \mu_{yx}^{(1)}/\mu_{yy}^{(1)}$  is the valley anisotropy factor. In what follows, we use the dimensionless variables  $\kappa_\alpha = n_\alpha/N$ ,  $\kappa_\pm = \kappa_1 \pm \kappa_2$ ,  $\zeta = y/d$ , and dimensionless electric field  $\mathcal{E}_{x,y} = E_{x,y}/E_d$ , where  $E_d = k_B T/ae_0 d$ ,  $k_B$  is the Boltzmann constant,  $e_0$  is the elementary electric charge ( $e_0 > 0$ ), and  $T$  is the temperature. Thus, Eqs. (12) and (13) are decoupled:

$$\frac{d^2\kappa_-}{d\zeta^2} - 3\mathcal{E}_x\kappa_- \frac{d\kappa_-}{d\zeta} + \mathcal{E}_x^2\kappa_-(\kappa_-^2 - 1) = 0, \quad (14)$$

$$\kappa_+ = \kappa_-^2 - \frac{1}{\mathcal{E}_x} \frac{d\kappa_-}{d\zeta}, \quad (15)$$

$$\mathcal{E}_y = -a\kappa_- \mathcal{E}_x. \quad (16)$$

The electron densities in different valleys are expressed through the solution of Eq. (14),  $\kappa_-(\zeta)$ , as

$$\begin{aligned} \kappa_1 &= \frac{1}{2} \left( \kappa_-^2 + \kappa_- - \frac{1}{\mathcal{E}_x} \frac{d\kappa_-}{d\zeta} \right), \\ \kappa_2 &= \frac{1}{2} \left( \kappa_-^2 - \kappa_- - \frac{1}{\mathcal{E}_x} \frac{d\kappa_-}{d\zeta} \right), \\ \kappa_3 &= 1 - \kappa_-^2 + \frac{1}{\mathcal{E}_x} \frac{d\kappa_-}{d\zeta}. \end{aligned} \quad (17)$$

The second-order differential nonlinear equation (14) does not contain the independent variable  $\zeta$  explicitly and includes one parameter  $\mathcal{E}_x$ . Noting that the equation is invariant under the change  $\zeta \rightarrow -\zeta$ ,  $\kappa_- \rightarrow -\kappa_-$ , the solution  $\kappa_- = \kappa_-(\zeta)$  is represented by an odd function of  $\zeta$ . In particular,  $n_{1,2}(-\zeta) = -n_{2,1}(\zeta)$  and  $n_3(-\zeta) = n_3(\zeta)$ . Note that the substitution  $\xi = \mathcal{E}_x \zeta$  transforms Eq. (14) to a universal form without parameters

$$\frac{d^2\kappa_-}{d\xi^2} - 3\kappa_- \frac{d\kappa_-}{d\xi} + \kappa_-(\kappa_-^2 - 1) = 0. \quad (18)$$

The solution is

$$\kappa_-(\xi) = -\frac{\sinh \xi}{b_0 + \cosh \xi}, \quad (19)$$

where  $b_0$  is an arbitrary constant (see Appendix A for details). Thereby, the explicit expressions have been found for the valley electron densities given in Eq. (17). The constant  $b_0$  is determined from the condition of conservation of the total number of carriers in each valley. The latter is equivalent to integration of the valley density  $n_\alpha(y)$  over the channel width

$$\int_{-d}^d n_\alpha(y) dy = 2dn_0. \quad (20)$$

For example, using  $n_3(y) = N - n_+(y)$  in (20), we obtain

$$\frac{1}{2} \int_{-1}^1 \kappa_+(\zeta; b_0, \mathcal{E}_x) d\zeta = \frac{2}{3}, \quad (21)$$

where  $\kappa_+(\xi; b_0, \mathcal{E}_x)$ , given in Eqs. (15) and (19), is

$$\kappa_+(\xi; b_0, \mathcal{E}_x) = \frac{\cosh \xi}{b_0 + \cosh \xi}, \quad (22)$$

and  $\xi = \mathcal{E}_x \zeta$ . After the substitution of  $\kappa_+$  of Eq. (22) in the left-hand side of Eq. (21), this equation reduces to a compact

form

$$b_0 \mathcal{I}(\mathcal{E}_x, b_0) = \frac{1}{3} \mathcal{E}_x, \quad (23)$$

where the integral

$$\mathcal{I}(\mathcal{E}_x, b_0) = \int_0^{\mathcal{E}_x} \frac{d\xi}{b_0 + \cosh \xi} \quad (24)$$

can be evaluated analytically [47]. Using this result, the approximate expression for  $b_0$  can be obtained in the limit of high fields ( $\mathcal{E}_x \gg 1$ )  $b_0 \simeq (1/2) \exp(\mathcal{E}_x/3)$ . Hence, the constant  $b_0 = b_0(\mathcal{E}_x)$  is calculated for a given value of the electric field  $\mathcal{E}_x$  from Eqs. (23) and (24) and thereby the valley electron densities

$$\begin{aligned} \frac{n_1}{N} &= \frac{1}{2} \frac{e^{-\xi}}{b_0 + \cosh \xi}, \\ \frac{n_2}{N} &= \frac{1}{2} \frac{e^{\xi}}{b_0 + \cosh \xi}, \\ \frac{n_3}{N} &= \frac{b_0}{b_0 + \cosh \xi}, \end{aligned} \quad (25)$$

as well as the transverse electric field

$$\mathcal{E}_y = a\mathcal{E}_x \frac{\sinh \xi}{b_0 + \cosh \xi}, \quad (26)$$

where  $\xi = \mathcal{E}_x \zeta$ . Figure 2 shows the results for valley electron densities [Figs. 2(a), 2(c), and 2(e)] and transverse induced electric field [Figs. 2(b), 2(d), and 2(f)] obtained by numerical calculation of Eqs. (25) and (26) for different values of dimensionless electric field  $\mathcal{E}_x$ . It is observed that for  $\mathcal{E}_x = 5$ , which is not appreciably higher than the characteristic diffusion field  $E_d$ , the transverse separation of the electrons of different valleys is already considerable so that one can state the formation of valley-polarized domains. Also, it is seen a clear tendency for domain structure to become more pronounced with increasing the magnitude of the applied electric field.

The valley-polarized domains result in efficient separation of the valley current densities across the nanostructure. Indeed, transverse distributions of the valley current densities in the direction of the applied electric field follow from Eq. (1):

$$J_x^{(1)} = (c_1 \mathcal{E}_x + \mathcal{E}_y) \kappa_1 + a \frac{d\kappa_1}{d\zeta}, \quad (27a)$$

$$J_x^{(2)} = (c_1 \mathcal{E}_x - \mathcal{E}_y) \kappa_2 - a \frac{d\kappa_2}{d\zeta}, \quad (27b)$$

$$J_x^{(3)} = c_3 \mathcal{E}_x \kappa_3, \quad (27c)$$

where  $J_x^{(\alpha)} = j_x^{(\alpha)}/j_c$ ,  $j_c = e_0 \mu_{xy}^{(1)} N E_d$  is the normalization current density, and  $c_\alpha = \mu_{xx}^{(\alpha)}/\mu_{xy}^{(1)}$  ( $c_1 = c_2$ ). Substituting  $\kappa_{1,2}$  and  $\mathcal{E}_y$  from Eqs. (25) and (26) into Eqs. (27a) and (27b), we reduce  $J_x^{(1,2)}$  to the form of  $J_x^{(3)}$  in Eq. (27c), that is,  $J_x^{(1,2)} = (c_1 - a) \mathcal{E}_x \kappa_{1,2}$  [Figs. 4(a) and 4(b)].

The total current density,  $j_x/j_c \equiv J_x = J_x^{(1)} + J_x^{(2)} + J_x^{(3)}$ , is obtained by the summation of valley current densities as  $J_x(\zeta) = \sigma(\mathcal{E}_x, \zeta) \mathcal{E}_x$ , where

$$\sigma(\mathcal{E}_x, \zeta) = [c_3 + (c_1 - c_3 - a) \kappa_+(\mathcal{E}_x, \zeta)]. \quad (28)$$

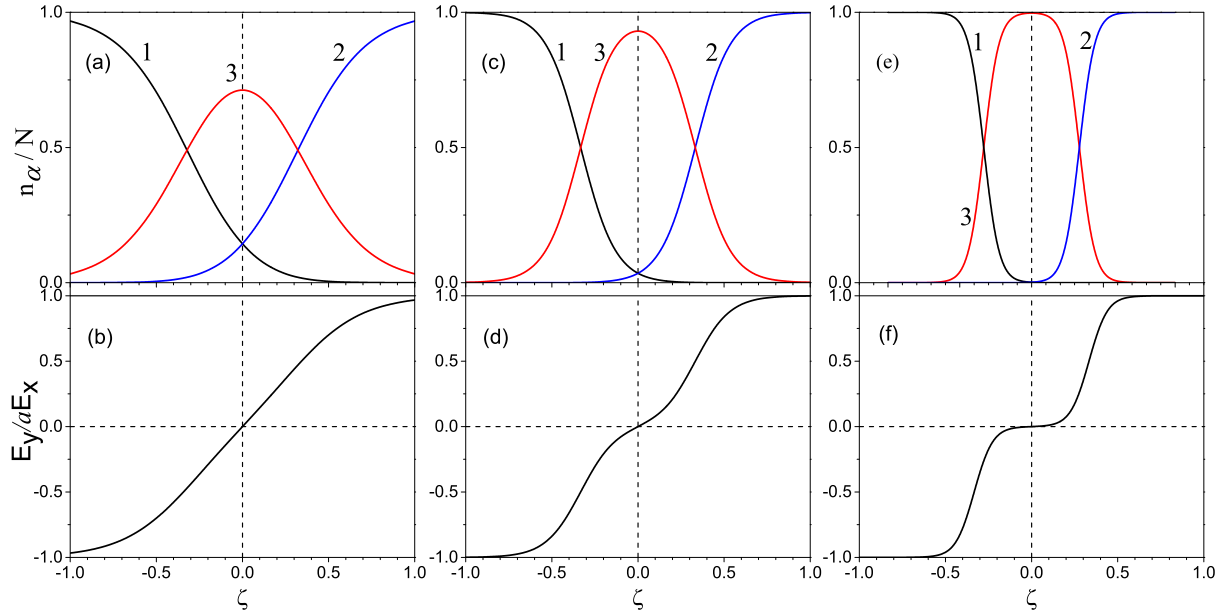


FIG. 2. Valley-polarized domains calculated by Eqs. (25) and (26) for different values of electric field  $\mathcal{E}_x$ : (a), (b)  $\mathcal{E}_x = 5$ , (c), (d) 10, (e), (f) 20. (a), (c), (e) Distributions of the valley electron density  $n_\alpha(\zeta)/N$ . The curves are 1 (black) valley 1, 2 (blue) valley 2, and 3 (red) valley 3. (b), (d), (f) Transverse distributions of the induced electric field (dimensional)  $\mathcal{E}_y(\zeta)/a\mathcal{E}_x$ .

We calculate the current density averaged over the sample width

$$\bar{j}_x = \frac{1}{2d} \int_{-d}^d j_x(y) dy.$$

The normalized average current density,  $\bar{J}_x = \bar{j}_x/j_c$ , is

$$\bar{J}_x = \left[ c_3 + (c_1 - c_3 - a) \frac{1}{2} \int_{-1}^1 \kappa_+(\zeta) d\zeta \right] \mathcal{E}_x. \quad (29)$$

Taking into account Eq. (21), we find  $\bar{J}_x = \bar{\sigma} \mathcal{E}_x$ , where  $\bar{\sigma} = (2c_1 + c_3 - 2a)/3$ . In the absence of the valley-polarized domains, all the valleys are equally populated so that the current density is  $J_x^{(0)} \equiv j_x^{(0)}/j_c = \bar{\sigma} \mathcal{E}_x$ , which is the consequence of symmetrical orientation of valleys relative to the edges.

As it has been noted in the Introduction section, another 2D electron system which is of interest here is represented by AIAs QWs with the growth direction along [001] ( $z$  axis), where the lowest two in-plane ( $x$  and  $y$ ) valleys are only occupied [21]. For nanostrips of the width  $2d$  with symmetrical orientation of the in-plane valleys relative to the nanostrip edges, this is an example of the simplest 2D multivalley system. In this case, the theory for the valley-polarized domain formation is developed in the same way as for the three-valley system analyzed in this section. As is evident from the main equations of Sec. III, the results for the two-valley case are obtained by setting the electron density  $n_3 = 0$  and the parameter  $b_0 = 0$ . Then, from Eqs. (19), (25), and (26) as well as the equations of Appendix A, we find that

$$\frac{n_1}{N} = \frac{e^{-\mathcal{E}_x \zeta}}{2 \cosh(\mathcal{E}_x \zeta)}, \quad \frac{n_2}{N} = \frac{e^{\mathcal{E}_x \zeta}}{2 \cosh(\mathcal{E}_x \zeta)}, \quad (30)$$

and the transverse electric field  $\mathcal{E}_y = a\mathcal{E}_x \tanh(\mathcal{E}_x \zeta)$ , also the valley polarization  $\kappa_- = -\tanh(\mathcal{E}_x \zeta)$  with  $\kappa_+ = 1$ . Thus, for the two-valley case which can be realized in the AIAs QW

nanostrips at high electric fields, the two domains of valley polarization occur separated by the single domain wall (compare with the three-valley domain structure depicted in Fig. 2).

#### IV. FINITE INTERVALLEY SCATTERING TIME

The continuity equations (6) for the considered group of valleys have the form

$$\begin{aligned} \frac{dj_y^{(1)}}{dy} &= -\frac{1}{\tau} (2n_1 - n_2 - n_3), \\ \frac{dj_y^{(2)}}{dy} &= -\frac{1}{\tau} (2n_2 - n_1 - n_3), \\ \frac{dj_y^{(3)}}{dy} &= -\frac{1}{\tau} (2n_3 - n_1 - n_2), \end{aligned} \quad (31)$$

where  $\tau$  is the intervalley scattering time. For a finite  $\tau$ , it is convenient to use the dimensionless variables

$$\mathcal{E}_{x,y} = \frac{E_{x,y}}{E_c}, \quad E_c = \frac{k_B T}{ae_0 L_{iv}}, \quad L_{iv} = (D_{yy}^{(1)} \tau / 2)^{1/2}, \quad \zeta = \frac{y}{L_{iv}}. \quad (32)$$

Then, Eqs. (31) can be written as

$$\begin{aligned} \frac{d}{d\zeta} \left( a^{-1} \kappa_1 \mathcal{E}_y + \kappa_1 \mathcal{E}_x + \frac{d\kappa_1}{d\zeta} \right) &= \frac{1}{2} (3\kappa_1 - 1), \\ \frac{d}{d\zeta} \left( a^{-1} \kappa_2 \mathcal{E}_y - \kappa_2 \mathcal{E}_x + \frac{d\kappa_2}{d\zeta} \right) &= \frac{1}{2} (3\kappa_2 - 1), \\ \frac{d}{d\zeta} \left( a^{-1} b \kappa_3 \mathcal{E}_y + b \frac{d\kappa_3}{d\zeta} \right) &= 1 - \frac{3}{2} (\kappa_1 + \kappa_2), \end{aligned} \quad (33)$$

where  $b = \mu_{yy}^{(3)}/\mu_{yy}^{(1)}$  and

$$\mathcal{E}_y = -a \frac{\mathcal{E}_x (\kappa_1 - \kappa_2) + d(\kappa_1 + \kappa_2)/d\zeta + b(d\kappa_3/d\zeta)}{\kappa_1 + \kappa_2 + b\kappa_3}. \quad (34)$$

The quasineutrality condition is expressed as

$$\kappa_1 + \kappa_2 + \kappa_3 = 1. \quad (35)$$

We note that the solutions to Eqs. (33)–(35) obey the following symmetry requirements:

$$\kappa_{1,2}(-\zeta) = \kappa_{2,1}(\zeta), \quad \kappa_3(-\zeta) = \kappa_3(\zeta), \quad \mathcal{E}_y(-\zeta) = -\mathcal{E}_y(\zeta). \quad (36)$$

Below, in the analysis, we consider for simplicity the intervalley scattering rates at the edges equal to zero ( $S_{\alpha\beta}^{\pm} = 0$ ). In this case, the BCs (7) to the continuity equations (33) are written as

$$\begin{aligned} \left( a^{-1} \mathcal{E}_y \kappa_1 + \mathcal{E}_x \kappa_1 + \frac{d\kappa_1}{d\zeta} \right)_{\pm\delta} &= 0, \\ \left( a^{-1} \mathcal{E}_y \kappa_2 - \mathcal{E}_x \kappa_2 + \frac{d\kappa_2}{d\zeta} \right)_{\pm\delta} &= 0, \\ \left( a^{-1} \mathcal{E}_y \kappa_3 + \frac{d\kappa_3}{d\zeta} \right)_{\pm\delta} &= 0. \end{aligned} \quad (37)$$

In terms of  $\kappa_{\pm} = \kappa_1 \pm \kappa_2$ , Eqs. (33) and (34) take the form

$$\begin{aligned} \frac{d}{d\zeta} \left( \mathcal{E}_x \kappa_- + a^{-1} \mathcal{E}_y \kappa_+ + \frac{d\kappa_+}{d\zeta} \right) &= \frac{3}{2} \kappa_+ - 1, \\ \frac{d}{d\zeta} \left( a^{-1} \mathcal{E}_y \kappa_- + \mathcal{E}_x \kappa_+ + \frac{d\kappa_-}{d\zeta} \right) &= \frac{3}{2} \kappa_-, \\ \frac{d}{d\zeta} \left( a^{-1} b \mathcal{E}_y \kappa_3 + b \frac{d\kappa_3}{d\zeta} \right) &= 1 - \frac{3}{2} \kappa_+, \end{aligned} \quad (38)$$

and

$$a^{-1} \mathcal{E}_y = -\frac{\mathcal{E}_x \kappa_- + (1-b)(d\kappa_+/d\zeta)}{b + (1-b)\kappa_+}. \quad (39)$$

The BCs of Eq. (37) become

$$\begin{aligned} \left( a^{-1} \mathcal{E}_y \kappa_+ + \mathcal{E}_x \kappa_- + \frac{d\kappa_+}{d\zeta} \right)_{\pm\delta} &= 0, \\ \left( a^{-1} \mathcal{E}_y \kappa_- + \mathcal{E}_x \kappa_+ + \frac{d\kappa_-}{d\zeta} \right)_{\pm\delta} &= 0, \\ \left( a^{-1} \mathcal{E}_y \kappa_3 + \frac{d\kappa_3}{d\zeta} \right)_{\pm\delta} &= 0. \end{aligned} \quad (40)$$

It is seen that the first two equations in (38) and (40), together with Eq. (39), contain only two variables  $\kappa_{\pm}$ , so that they are separated from the third equation for the  $\kappa_3$  variable. Therefore, in the analysis provided below, we may consider the domain formation associated with the group of valleys 1 and 2, and the valley 3 separately. First, we analyze the domains arising from the valleys 1 and 2.

*Domain walls.* Approximate solutions describing the domain walls are obtained by considering the first and third terms on the left-hand side of first two equations in (38) as the major contribution while neglecting all remainder terms to obtain

$$\begin{aligned} \frac{d}{d\zeta} \left( \mathcal{E}_x \kappa_- + \frac{d\kappa_+}{d\zeta} \right) &= 0, \\ \frac{d}{d\zeta} \left( \mathcal{E}_x \kappa_+ + \frac{d\kappa_-}{d\zeta} \right) &= 0. \end{aligned} \quad (41)$$

This is the system of two differential equations of the second order which general solution contains four integration constants. The first two integrals are

$$\begin{aligned} \mathcal{E}_x \kappa_- + \frac{d\kappa_+}{d\zeta} &= C_+, \\ \mathcal{E}_x \kappa_+ + \frac{d\kappa_-}{d\zeta} &= C_-, \end{aligned} \quad (42)$$

where  $C_{\pm}$  are integration constants. Using the second equation,  $\kappa_+$  can be excluded in the first equation by the substitution

$$\kappa_+ = \frac{C_-}{\mathcal{E}_x} - \frac{1}{\mathcal{E}_x} \frac{d\kappa_-}{d\zeta}, \quad (43)$$

which results in a second-order linear differential equation with constant coefficients

$$\frac{d^2 \kappa_-}{d\zeta^2} - \mathcal{E}_x^2 \kappa_- = -\mathcal{E}_x C_+. \quad (44)$$

The solution of Eq. (44) is

$$\kappa_-(\zeta) = C_1 e^{\mathcal{E}_x \zeta} + C_2 e^{-\mathcal{E}_x \zeta} + \frac{C_+}{\mathcal{E}_x}, \quad (45)$$

where  $C_{1,2}$  are additional integration constants. Substituting  $\kappa_-(\zeta)$  from (45) into (43), we obtain

$$\kappa_+(\zeta) = \frac{C_-}{\mathcal{E}_x} - (C_1 e^{\mathcal{E}_x \zeta} - C_2 e^{-\mathcal{E}_x \zeta}). \quad (46)$$

Since the valley electron densities  $\kappa_{1,2}$  are expressed as  $\kappa_{1,2} = \frac{1}{2}(\kappa_+ \pm \kappa_-)$ , we find

$$\begin{aligned} \kappa_1(\zeta) &= \frac{C_- + C_+}{2\mathcal{E}_x} + C_2 e^{-\mathcal{E}_x \zeta}, \\ \kappa_2(\zeta) &= \frac{C_- - C_+}{2\mathcal{E}_x} - C_1 e^{\mathcal{E}_x \zeta}. \end{aligned} \quad (47)$$

For convenience, we redesignate the integration constants as follows:

$$\begin{aligned} A_1 &= \frac{C_+ + C_-}{2}, \quad A_2 = \frac{C_+ - C_-}{2}, \\ C_1 &= -e^{\mathcal{E}_x \zeta_2}, \quad C_2 = e^{\mathcal{E}_x \zeta_1} \end{aligned}$$

to obtain

$$\begin{aligned} \kappa_1(\zeta) &= e^{-\mathcal{E}_x(\zeta - \zeta_1)} + \frac{A_1}{\mathcal{E}_x}, \\ \kappa_2(\zeta) &= e^{\mathcal{E}_x(\zeta - \zeta_2)} - \frac{A_2}{\mathcal{E}_x}; \end{aligned} \quad (48)$$

here,  $\zeta_{1,2}$  determine the position of domain's wall,  $\zeta_1 < 0$  ( $\zeta_1 = -\zeta_2$ ,  $\zeta_2 > 0$ ),  $A_2 = -A_1$ . The latter follows from the symmetry properties reflected in Eq. (36).

The constants  $A_{1,2}$  can be found from the BCs of Eq. (37) for  $\kappa_1(\zeta)$  at  $\zeta = \delta$ , and for  $\kappa_2(\zeta)$  at  $\zeta = -\delta$ . Here, we use approximate expressions for the transverse electric field  $\mathcal{E}_y(\zeta = \pm\delta) \approx \pm a \mathcal{E}_x$  by utilizing in Eq. (39)  $\kappa_1 \approx 0$ ,  $\kappa_2 \approx 1$  at  $\zeta = \delta$ , and  $\kappa_2 \approx 0$ ,  $\kappa_1 \approx 1$  at  $\zeta = -\delta$ . Then, we find

$$\begin{aligned} \kappa_1(\zeta) &= e^{-\mathcal{E}_x(\zeta - \zeta_1)} - \frac{1}{2} e^{-\mathcal{E}_x(\delta - \zeta_1)}, \\ \kappa_2(\zeta) &= e^{\mathcal{E}_x(\zeta - \zeta_2)} - \frac{1}{2} e^{-\mathcal{E}_x(\delta + \zeta_2)}. \end{aligned} \quad (49)$$

In particular, using Eq. (49), we obtain

$$\kappa_+(\zeta) = 2e^{\mathcal{E}_x\zeta_1} \cosh(\mathcal{E}_x\zeta), \quad \kappa_-(\zeta) = -2e^{\mathcal{E}_x\zeta_1} \sinh(\mathcal{E}_x\zeta), \quad (50)$$

where we have used that  $\zeta_2 = -\zeta_1$ . Note that in the regions near the edges, where the contribution of the third valley is suppressed, the valley polarization  $P(\zeta)$  can be calculated as

$$P(\zeta) \approx P_{12}(\zeta) \equiv \frac{\kappa_-(\zeta)}{\kappa_+(\zeta)} = -\tanh(\mathcal{E}_x\zeta). \quad (51)$$

The characteristic length scale for the considered domain walls is the *compressed* intervalley diffusion length  $L_{\text{com}} = L_{\text{iv}}/\mathcal{E}_x \propto \mathcal{E}_x^{-1}$ .

*Domain plateaus.* As an example to be specific, we consider the formation of domain plateau near the edge  $y = d$ . The edge  $y = -d$  is analyzed in the same way. The transverse electric field in the plateau region follows from Eq. (39) where we can approximate  $\kappa_+(\zeta) \approx 1$  ( $\kappa_1 \approx 1, \kappa_2 \approx 0$ ) to obtain  $\mathcal{E}_y(\zeta) \approx -a\mathcal{E}_x\kappa_-(\zeta)$ . The substitution of  $\mathcal{E}_y(\zeta)$  into the second of Eqs. (38) results in equation for  $\kappa_-(\zeta)$  in the plateau region

$$\frac{d\kappa_-^2}{d\zeta} + \frac{3}{2\mathcal{E}_x}\kappa_- = 0. \quad (52)$$

The solution is

$$\kappa_-(\zeta) = -\frac{3}{4\mathcal{E}_x}(\zeta - \zeta_1) + C. \quad (53)$$

The integration constant  $C$  can be found from the second equation of the BCs (37) at the edge  $\zeta = -\delta$ ,

$$C = 1 - \frac{3}{4\mathcal{E}_x^2} - \frac{3}{4\mathcal{E}_x}(\delta + \zeta_1). \quad (54)$$

Thus, we obtain for the considered plateau

$$\kappa_-(\zeta) = 1 - \frac{3}{4\mathcal{E}_x^2} - \frac{3}{4\mathcal{E}_x}(\delta + \zeta). \quad (55)$$

The characteristic length scale for the domain plateaus is the *extended* intervalley diffusion length  $L_{\text{ext}} = L_{\text{iv}}\mathcal{E}_x \propto \mathcal{E}_x$ . For strong fields ( $\mathcal{E}_x \gg 1$ ), the approximate values of  $\kappa_-(\zeta)$  at the edges are  $\kappa_-(\pm\delta) \approx \mp 1$ .

*The central domain.* The central region of the total domain pattern is in-between the domain walls of the valleys 1 and 2, which are localized at  $\zeta = \zeta_1$  and  $\zeta_2$ , respectively. Since the carriers of the valleys 1 and 2 move from the sample bulk to the edges, this region is occupied mainly by the carriers of the valley 3, described by the dependence  $\kappa_3 = \kappa_3(\zeta)$  in accordance with the quasineutrality condition (35). Equation for the valley density  $\kappa_3(\zeta)$  is given in (38) where  $\mathcal{E}_y(\zeta)$  of Eq. (34) is expressed as

$$\mathcal{E}_y = -a \frac{\mathcal{E}_x\kappa_- + (d\kappa_+/d\zeta) + b(d\kappa_3/d\zeta)}{\kappa_+ + b\kappa_3}. \quad (56)$$

Here, using  $\kappa_{\pm}$  of Eq. (50), which results in that

$$\mathcal{E}_x\kappa_- + \frac{d\kappa_+}{d\zeta} = 0, \quad (57)$$

we can simplify  $\mathcal{E}_y$  of Eq. (56) as

$$\mathcal{E}_y = -\frac{ab}{\kappa_+ + b\kappa_3} \frac{d\kappa_3}{d\zeta}. \quad (58)$$

Substituting  $\mathcal{E}_y$  in (58) into the third equation in (38), we get

$$b \frac{d}{d\zeta} \left( \frac{\kappa_+}{\kappa_+ + b\kappa_3} \frac{d\kappa_3}{d\zeta} \right) = 1 - \frac{3}{2}\kappa_+. \quad (59)$$

Noting that  $\kappa_+(\zeta)$  is an even function of  $\zeta$ , we may conclude that Eq. (59) is invariant under the change of  $\zeta$  to  $-\zeta$  for an even function  $\kappa_3(\zeta) = \kappa_3(-\zeta)$ . Calculating the derivative in Eq. (59) and taking into account  $\kappa_3'(\zeta = 0) = 0$  at an extremum point, we obtain

$$b \frac{\kappa_+}{\kappa_+ + b\kappa_3} \kappa_3'' = 1 - \frac{3}{2}\kappa_+, \quad (60)$$

where  $1 - 3\kappa_+/2 > 0$  in the vicinity of  $\zeta = 0$ , and thus  $\kappa_3''(\zeta = 0) > 0$ . The latter means that  $\zeta = 0$  is the minimum point of the function  $\kappa_3 = \kappa_3(\zeta)$ . The formation of such a minimum can be explained by counter drift flows of the carriers of valley 3 from periphery regions to the center of the sample in the transverse electric field.

## V. DISCUSSIONS

In the preceding sections, the theory of valley-polarized domains has been developed in 2D multivalley semiconductor electron systems exhibiting anisotropic valley transport. More specifically, the electrical valley anisotropy is considered to be caused by valley-dependent anisotropic effective-mass energy spectra; examples are *n*-Si and *n*-AlAs based quantum nanostructures (in bulk materials, the effective-mass ratio  $m_l/m_t$  is 3.5 and 5.2, respectively).

In a nanostrip geometry with a finite width, the valley-polarized domain structure is formed under an applied in-plane electric field along the strip which causes the carriers of anisotropic valleys to flow toward the opposite edges where they accumulate, creating well-resolved spatial regions (domains) of strong valley polarization. In the case of 2D electrons on Si(111) surface considered in this work, the domain structure consists of three space domains occupied with the electrons of only one valley in accordance with the effective many-valley band structure. This is illustrated qualitatively by Fig. 1 as well as demonstrated with numerical calculations presented in Figs. 2 and 3. Typically, for strong field  $E_x > E_c$ , the domain regions are characterized by the plateau of a smooth coordinate behavior and the wall of an abrupt coordinate behavior. The two different length scales determine the extent of the domain plateau  $L_{\text{ext}} = L_c E_x / E_c$  and the domain wall  $L_{\text{com}} = L_c E_c / E_x$ , with the contrast ratio  $L_{\text{ext}}/L_{\text{com}} = (E_x/E_c)^2 \gg 1$ . The characteristic length  $L_c = L_{\text{iv}}$  and the electric field  $E_c = k_B T / a e_0 L_{\text{iv}}$  are given in Eq. (32) for the case of a finite intervalley scattering time  $\tau$ . If the intervalley scattering is very weak ( $\tau \rightarrow \infty$ ), then  $L_{\text{ext}} = d$  and in the expressions for  $L_{\text{com}}$  and  $E_c$ , the intervalley scattering length  $L_{\text{iv}}$  is changed by  $d$ . With increasing the applied electric field, the domain structure becomes more resolved. This is clearly demonstrated in Fig. 2 where the results of numerical calculations of valley-polarized domains are presented for several values of  $\mathcal{E}_x$ . For example, for  $\mathcal{E}_x = 10$ , we obtain  $L_{\text{ext}}/L_{\text{com}} = 100$  which shows that the domain wall constitutes only 1% of the domain plateau.

The valley-polarized domain formation results in the appropriate separation of the valley currents across the nanostrip width, which flow along the nanostrip mostly in the space

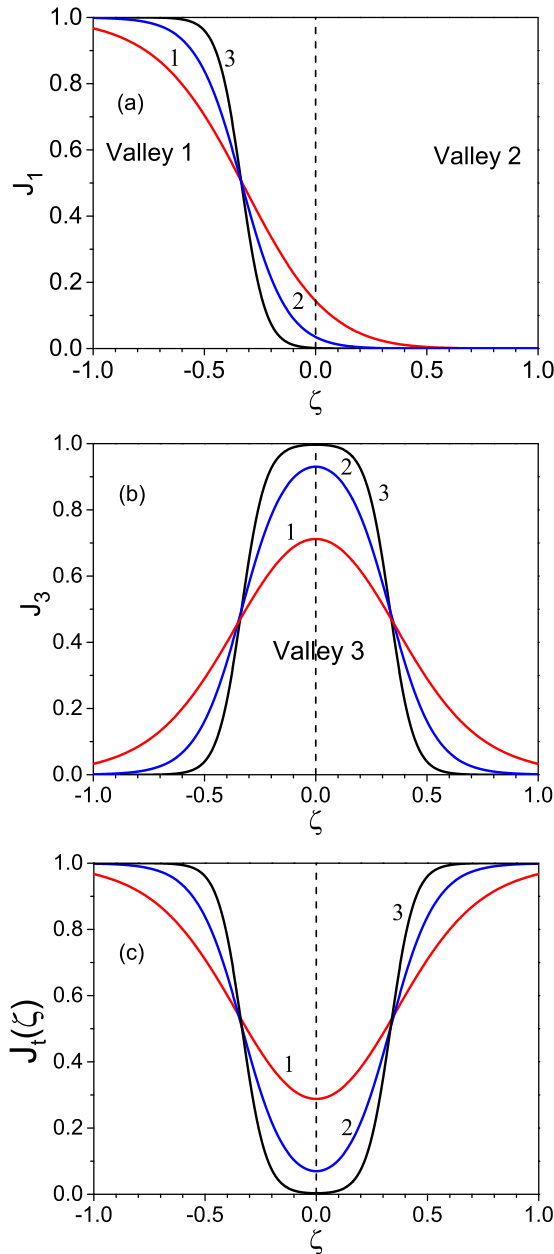


FIG. 3. Transverse distributions of the current density calculated for different values of  $\mathcal{E}_x$ . The curves are 1 (red)  $\mathcal{E}_x = 5$ ; 2 (blue), 10; and 3 (black), 20. (a) Distributions of the current density of valley 1,  $J_1(\zeta) = J_x^{(1)}(\zeta)/(c_1 - a)\mathcal{E}_x$ . The current density distributions of valley 2 are localized at the opposite edge  $\zeta = 1$  (not shown) obtained by inversion of the curves 1–3 relative to vertical dashed line  $\zeta = 0$ . (b) Distributions of the current density of valley 3,  $J_3(\zeta) = J_x^{(3)}(\zeta)/c_3\mathcal{E}_x$ . (c) Distributions of the total current density  $J_i(\zeta) = J_x(\zeta)/\mathcal{E}_x - [c_3/(c_1 - c_3 - a)]$ .

regions of each valley-polarized domain localization. Such valley filamentation of the electron current density in the nanostrip with valley-polarized domains is illustrated in Fig. 3, where we show distributions of the valley current densities [Figs. 3(a) and 3(b)] together with the total current density [Fig. 3(c)] calculated for the same values of  $\mathcal{E}_x$  as in Fig. 2.

In the domain wall where the electric field  $E_y(y)$  can vary rapidly (Fig. 2), one may expect accumulation of

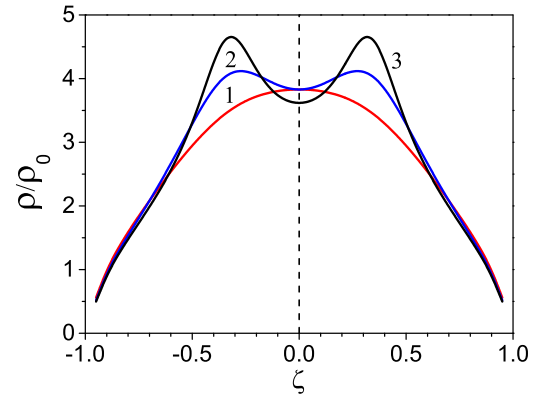


FIG. 4. Transverse distributions of the local charge density  $\varrho(\zeta)/\varrho_0$  calculated for different values of  $\mathcal{E}_x$ ;  $\varrho_0 = 4e_0N(L_D/d)\mathcal{E}_x$ . The curves are 1 (red)  $\mathcal{E}_x = 5$ ; 2 (blue), 10; and 3 (black), 20.

electric charges such that the condition of quasineutrality used in this work [Eqs. (11) and (35)] may not be obeyed. The induced electric charge can be estimated from the solution of the Poisson equation (Appendix B). Distributions of the induced electric charge density calculated for different values of  $\mathcal{E}_x$  are presented in Fig. 4. The obtained correction  $\delta\kappa \sim (L_D/d)\mathcal{E}_x$  is small in the smallness of the inverse aspect ratio  $(L_D/d) \ll 1$ , where  $L_D$  is the screening length. This justifies the quasineutrality condition. For order-of-magnitude numerical estimations, we take the electron density  $N = 10^{11} \text{ cm}^{-2}$ , the dielectric constant  $\varepsilon_0 = 11.6$ ,  $\varepsilon = (\varepsilon_0 + 1)/2 = 6.3$ ,  $T = 77 \text{ K}$ , and  $d = 0.5 \times 10^{-4} \text{ cm}$ . Then we obtain  $L_D = 0.2 \times 10^{-6} \text{ cm}$ ,  $L_D/d = 4 \times 10^{-3}$ , and for  $\mathcal{E}_x = 10$  the induced electric charge density  $\delta\kappa \sim (L_D/d)\mathcal{E}_x = 4 \times 10^{-2}$ . Note, spatial distributions of charges and electrostatic potentials on nanoscale can be studied using different scanning microscopic methods. For example, nanometer-scale imaging of the surface potential can be received with the Kelvin probe force microscopy [48].

It is interesting to note that under the valley-polarized domains, the current density  $J_x = J_x(\zeta)$  in Eq. (28) is dependent on the transverse coordinate  $\zeta$  [Fig. 4(c)]. Such dependence leads to the appearance of a nontrivial magnetic field component  $H_z$ , normal to the nanostructure plane, in addition to the trivial  $H_y$  component ( $H_x = 0$ ). Using the Maxwell equations  $\nabla \cdot \mathbf{H} = 0$  and  $\nabla \times \mathbf{H} = (4\pi/c)\mathbf{j}$ , the equation for  $H_z$  has been derived and its solution has been found (Appendix C). The function  $H_z = H_z(y, z)$  of the two variables  $(y, z)$  has the following properties:  $H_z(-y, z) = -H_z(y, z)$  and  $H_z(y = 0, z) = 0$ . It is observed that the magnetic field  $H_z$  is concentrated mainly within the valley-polarized domains (i.e., the domain plateaus), where  $H_z$  takes opposite signs and approaches zero in the region of the domain wall. Scanning of the magnetic field distributions near the nanostrip surface [49] may allow to observe the valley-polarized domain formation.

## VI. SUMMARY

In this work, we have investigated the formation of electrically induced valley-polarized domains in 2D conducting channels of a nanostrip with finite width  $\lesssim L_{iv}$  ( $L_{iv}$  is the



intervalley diffusion length) made of many-valley semiconductors with equivalent anisotropic valleys such as  $n$ -Si or  $n$ -AlAs. The domains are well-resolved spatial regions in which the electrons of only one valley are present, thereby allowing the valley degree of freedom to be accessed independently. The domains are developed in the transverse direction relative to the applied electric field due to the electron flows of anisotropic valleys onto the opposite nanostrip edges. The valley-polarized domains can appear at the field strength  $E \gg E_c$ , where  $E_c$  is the characteristic diffusion field. They are characterized by extensive plateaus of the order of  $L_{\text{ext}} = L_{\text{iv}}E/E_c$  and a narrow wall of the order of  $L_{\text{com}} = L_{\text{iv}}E_c/E$ . (In the absence of intervalley scattering, the intervalley diffusion length is replaced by the nanostrip width.) Since the domain wall is very narrow ( $\sim 1\%$  of the domain width), the carriers are fully valley polarized which enables a pure bulk valley current inside the considered domain region. The calculation shows that in the region of the domain wall, the induced electric field is rapidly varying, which results in the appearance of an excess electric charge beyond the local quasineutrality condition. The correction associated with the built-in electric charge density is small in the smallness of the inverse aspect ratio  $\sim L_D/d \ll 1$  ( $L_D$  is the screening length). Since the valley-polarized domain patterns are accompanied by space redistributions of the valley current densities across the nanostrip, the net current density becomes inhomogeneous, i.e., dependent on the transverse coordinate. As a consequence, magnetic domains with magnetic field normal to the nanostrip plane are formed where the induced magnetic field is concentrated mostly in the region of valley-polarized domain plateau. Experimental verification of the studied valley-polarized domains can be done by utilizing the existing methodologies focused on the spatial dependence of electrical, optical, and magnetic properties and their nanometer-scale imaging.

We suggest that the study of electrically induced domains of valley polarization in 2D nanosystems brings new knowledge on valley physics and can be used in valleytronics applications.

#### ACKNOWLEDGMENT

Authors of this paper have maintained scientific contacts with Prof. E. I. Rashba during many years and appreciated his influence upon their research activity, as well as his strong impact on the formation and development of modern condensed matter theory in Ukraine.

#### APPENDIX A: ANALYTICAL SOLUTION OF THE NONLINEAR DRIFT-DIFFUSION EQUATIONS

The second-order nonlinear differential equation (18) has been derived from Eqs. (10) which can be written in dimensionless form as

$$\begin{aligned} \frac{d\kappa_1}{d\xi} &= (\kappa_- - 1)\kappa_1, \\ \frac{d\kappa_2}{d\xi} &= (\kappa_- + 1)\kappa_2, \\ \frac{d\kappa_3}{d\xi} &= \kappa_- \kappa_3. \end{aligned} \quad (\text{A1})$$

These equations can be formally integrated, considering  $\kappa_-(\xi)$  as a given function of  $\xi$ ,

$$\begin{aligned} \kappa_1(\xi) &= C_1 e^{-\xi + \mathcal{I}(\xi)}, \\ \kappa_2(\xi) &= C_2 e^{\xi + \mathcal{I}(\xi)}, \\ \kappa_3(\xi) &= C_3 e^{\mathcal{I}(\xi)}, \end{aligned} \quad (\text{A2})$$

where  $\mathcal{I}(\xi) = \int_0^\xi \kappa_-(\xi') d\xi'$  and  $C_\alpha$  ( $\alpha = 1, 2, 3$ ) are integration constants. We note that in the limit of weak intervalley scattering ( $\tau \rightarrow \infty$ ,  $S_{\alpha\beta}^\pm \rightarrow 0$ ), the solutions  $\kappa_\alpha$  given in Eqs. (A2) satisfy the BCs (7) identically. The integration constants  $C_\alpha$  can be determined as follows. Taking into account that  $\kappa_-(\xi)$  is an odd function of  $\xi$ , so that  $\kappa_-(\xi = 0) = 0$ , we obtain  $C_1 = C_2 \equiv C$ . In addition, from the quasineutrality condition (11) of the form

$$\kappa_1(\xi) + \kappa_2(\xi) + \kappa_3(\xi) = 1, \quad (\text{A3})$$

it follows that, for  $\xi = 0$ ,  $C_1 + C_2 + C_3 = 1$ . Then, we express  $C_3 = 1 - 2C$ . Thus, Eqs. (A2) become

$$\begin{aligned} \kappa_1(\xi) &= C e^{-\xi + \mathcal{I}(\xi)}, \\ \kappa_2(\xi) &= C e^{\xi + \mathcal{I}(\xi)}, \\ \kappa_3(\xi) &= (1 - 2C) e^{\mathcal{I}(\xi)}. \end{aligned} \quad (\text{A4})$$

We substitute  $\kappa_\alpha(\xi)$  of Eqs. (A4) in Eq. (A3) and solve for the integral  $\mathcal{I}(\xi)$  to obtain

$$\mathcal{I}(\xi) = -\ln[1 + 2C(\cosh \xi - 1)]. \quad (\text{A5})$$

Since  $\kappa_-(\xi) [= \kappa_1(\xi) - \kappa_2(\xi)]$  is expressed from Eqs. (A4) as

$$\kappa_-(\xi) = -2C e^{\mathcal{I}(\xi)} \sinh \xi, \quad (\text{A6})$$

making use of Eq. (A5), we finally find

$$\kappa_-(\xi) = -2C \frac{\sinh \xi}{(1 - 2C) + 2C \cosh \xi}. \quad (\text{A7})$$

It is seen from the direct comparison that Eq. (A7) coincides with Eq. (19), with  $a_0 = 2C$  and  $b_0 = (1 - a_0)/a_0$ . The integration constant  $C$  (or, equivalently,  $b_0$ ) can be found from the condition of conservation of the total number of carriers in each valley, noted in Eq. (20).

#### APPENDIX B: THE POISSON EQUATION

Since the conducting channel is homogeneous in the  $x$  direction, we can proceed with the 2D Poisson equation

$$\frac{\partial^2 \phi}{\partial y^2} + \frac{\partial^2 \phi}{\partial z^2} = -\frac{4\pi}{\epsilon_0} \rho(y) \delta(z), \quad (\text{B1})$$

where  $\phi = \phi(y, z)$  is the electrostatic potential,  $\rho(y) = e_0[N - n(y)]$  is the electric charge density,  $n(y)$  is the local electron density,  $\epsilon_0$  is the dielectric constant, and  $\delta(z)$  is the delta function. We omit the dependence on  $x$  coordinate in  $\phi$ , which is set up with the applied voltage. Such assumption can be justified [50] by analyzing the reduced potential resulting from three-dimensional (3D) potential by integration on the  $x$  coordinate within the longest sample dimension  $d_x \gg (d_y, d_z)$  ( $|z| \lesssim d_z$ ).

It is convenient to use the dimensionless quantities  $\Phi = e_0 \phi / k_B T$ ,  $\zeta = y/d$ ,  $\eta = z/d$ , and  $\kappa = n/N$ . The solution  $\Phi =$

$\Phi(\zeta, \eta)$  to Eq. (B1) is expressed in standard form [51] with the aid of the 2D Green function [50]

$$G(\zeta - \zeta', \eta - \eta') = -\frac{1}{2\pi} \ln[(\zeta - \zeta')^2 + (\eta - \eta')^2]^{1/2}. \quad (\text{B2})$$

The result is

$$\Phi(\zeta, \eta) = -\frac{d}{(2\pi)^2 L_D} \int_{-1}^1 \delta\kappa(\zeta') \ln[(\zeta - \zeta')^2 + \eta^2]^{1/2} d\zeta', \quad (\text{B3})$$

where  $\delta\kappa(\zeta) = 1 - \kappa(\zeta)$  and  $L_D = \varepsilon_0 k_B T / 4\pi e_0^2 N$  is the screening length. The induced electric field [ $E_y = -\partial\phi(y, z)/\partial y$ ,  $E_z = -\partial\phi(y, z)/\partial z$ ] is expressed in dimensionless form as

$$\mathcal{E}_y(\zeta, \eta) = \frac{ad}{(2\pi)^2 L_D} \int_{-1}^1 \delta\kappa(\zeta') \frac{\zeta - \zeta'}{(\zeta - \zeta')^2 + \eta^2} d\zeta', \quad (\text{B4a})$$

$$\mathcal{E}_z(\zeta, \eta) = \frac{ad}{(2\pi)^2 L_D} \int_{-1}^1 \delta\kappa(\zeta') \frac{\eta}{(\zeta - \zeta')^2 + \eta^2} d\zeta'. \quad (\text{B4b})$$

The field components  $\mathcal{E}_{y,z}(\zeta, \eta)$  as functions of two variables  $(\zeta, \eta)$  have the following properties:  $\mathcal{E}_y(-\zeta, \eta) = -\mathcal{E}_y(\zeta, \eta)$ ,  $\mathcal{E}_y(\zeta, -\eta) = \mathcal{E}_y(\zeta, \eta)$  and  $\mathcal{E}_z(-\zeta, \eta) = \mathcal{E}_z(\zeta, \eta)$ ,  $\mathcal{E}_z(\zeta, -\eta) = -\mathcal{E}_z(\zeta, \eta)$ . From Eq. (B4a), the induced in-plane electric field is given by

$$\mathcal{E}_y(\zeta, \eta = 0) = \frac{ad}{(2\pi)^2 L_D} \int_{-1}^1 \frac{\delta\kappa(\zeta')}{\zeta - \zeta'} d\zeta'. \quad (\text{B5})$$

We note that the electrostatic equations must be integrated self-consistently with the transport equations, which is a complex computational problem. Here, as an alternative, we exploit the iterative procedure based on small aspect ratio ( $L_D/d_y \ll 1$ ). Using  $\mathcal{E}_y(\zeta)$  given in Eq. (16) and  $\mathcal{E}_y(\zeta, \eta = 0)$  of Eq. (B5) in the condition  $\mathcal{E}_y(\zeta, \eta = 0) = \mathcal{E}_y(\zeta)$ , we obtain an integral equation for the induced electric charge  $\delta\kappa(\zeta)$ :

$$\frac{1}{(2\pi)^2} \int_{-1}^1 \frac{\delta\kappa(\zeta')}{\zeta - \zeta'} d\zeta' + \frac{L_D}{d} \kappa_-(\zeta) \mathcal{E}_x = 0, \quad (\text{B6})$$

where  $\kappa_-(\zeta)$  is given in Eq. (19). Then it follows that  $\delta\kappa(-\zeta) = \delta\kappa(\zeta)$ . The integral in Eq. (B6) is understood in the principal sense [52]. Its solution, bounded at both ends  $\zeta = \pm 1$ , calculated for different values of  $\mathcal{E}_x$  is shown in Fig. 4. The induced electric charge  $\delta\kappa(\zeta)$  characterizes the extent of deviation from the local quasineutrality condition  $\kappa(\zeta) = 1$ . The results demonstrate that  $\delta\kappa(\zeta)$  in the vicinity of its maximum values is of the order of  $\delta\kappa \sim (L_D/d) \mathcal{E}_x$ , and for the assumed values of the accepted parameters it is small in the smallness of the inverse aspect ratio ( $L_D/d \ll 1$ ). This justifies the quasineutrality condition used in the work.

The spatial distributions of electrostatic potential  $\Phi(\zeta, \eta)$  and electric field  $\{\mathcal{E}_y(\zeta, \eta), \mathcal{E}_z(\zeta, \eta)\}$  can be calculated with the substitution of  $\delta\kappa(\zeta)$  into Eqs. (B3), (B4a), and (B4b), respectively.

### APPENDIX C: GENERATION OF MAGNETIC FIELD NORMAL TO THE NANOLAYER

The appearance of the magnetic field perpendicular to the nanostructure plane (Fig. 1), generated by the inhomogeneous current density  $j_x(y)$ , follows from the Maxwell equations

$$\nabla \cdot \mathbf{H} = 0, \quad \nabla \times \mathbf{H} = \frac{4\pi}{c} \mathbf{j}. \quad (\text{C1})$$

Operating with the gradient  $\nabla \times$  on both sides of the second equation and making use of the identity  $\nabla \times \nabla \times \mathbf{H} = \nabla(\nabla \cdot \mathbf{H}) - \Delta \mathbf{H}$ , with  $\nabla \cdot \mathbf{H} = 0$ , we obtain

$$\Delta \mathbf{H} = -\frac{4\pi}{c} \nabla \times [\mathbf{j} \delta(z)], \quad (\text{C2})$$

where  $\delta(z)$  takes into account in-plane character of the current density  $\mathbf{j} = \{j_x(y), 0\}$ . From Eq. (C2), we have derived the equation for the magnetic field component  $H_z$ :

$$\frac{\partial^2 H_z}{\partial y^2} + \frac{\partial^2 H_z}{\partial z^2} = \frac{4\pi}{c} \frac{\partial j_x}{\partial y} \delta(z). \quad (\text{C3})$$

This is a second-order partial differential equation with the 2D Laplace operator on the left-hand side acting on  $H_z = H_z(y, z)$ . Remarkably, this equation formally coincides with the Poisson equation (B1) analyzed in Appendix B. Therefore, its solution can be obtained using the same procedure employed therein. Thus, we find

$$\mathcal{H}_z(\zeta, \eta) = \frac{1}{4} \int_{-1}^1 \frac{\partial J_x(\zeta')}{\partial \zeta'} \ln[(\zeta - \zeta')^2 + \eta^2] d\zeta', \quad (\text{C4})$$

where we have used the dimensionless variables  $\zeta = y/d_y$ ,  $\eta = z/d_y$ , and  $\mathcal{H}_z = cH_z/2j_c$ . It is seen from Eq. (C4) that in case of a homogeneous current density,  $j_x(y) = \text{const}$ , the magnetic field  $H_z = 0$ . For the purposes of integration, we use the integration by parts which results in the expression

$$\mathcal{H}_z(\zeta, \eta) = \frac{1}{4} J_x(\mathcal{E}_x) \ln \left| \frac{(\zeta - 1)^2 + \eta^2}{(\zeta + 1)^2 + \eta^2} \right| + \frac{1}{2} \int_{-1}^1 J_x(\zeta') \frac{\zeta - \zeta'}{(\zeta - \zeta')^2 + \eta^2} d\zeta', \quad (\text{C5})$$

where  $J_x(\mathcal{E}_x) = J_x(|\zeta| = 1)$  is the longitudinal current density at the edges,

$$J_x(\mathcal{E}_x) = [c_3 + (c_1 - c_3 - a)\kappa_+(\mathcal{E}_x)] \mathcal{E}_x \quad (\text{C6})$$

and

$$\kappa_+(\mathcal{E}_x) = \frac{\cosh \mathcal{E}_x}{b_0 + \cosh \mathcal{E}_x}. \quad (\text{C7})$$

Equations (C6) and (C7) follow from Eqs. (28) and (22) with  $|\zeta| = 1$ , respectively.

- [1] A complete list of É. I. Rashba publications is available in [http://www.mit.edu/~levitov/rashba\\_papers/](http://www.mit.edu/~levitov/rashba_papers/).
- [2] É. I. Rashba, Redistribution of carriers between valleys in an electric field, *Sov.–Phys. JETP* **21**, 954 (1965) [*Zh. Eksp. Teor. Fiz.* **48**, 1427 (1965)].
- [3] Z. S. Gribnikov, V. A. Kochelap, and É. I. Rashba, Appearance of domains in “many-valley” semiconductors during the passage of strong currents, *Sov. Phys.–JETP* **24**, 178 (1967) [*Zh. Eksp. Teor. Fiz.* **51**, 266 (1966)].
- [4] É. I. Rashba, V. A. Romanov, I. I. Boiko, and I. P. Zhadko, Electrical pinch in elastically deformed germanium, *Phys. Status Solidi B* **16**, 43 (1966).
- [5] Z. S. Gribnikov, V. A. Kochelap, and É. I. Rashba, Domain structure of a multi-valley semiconductor in case of large currents, *Sov. Phys.–Solid State* **8**, 1981 (1967) [*Fiz. Tverd. Tela* **8**, 2479 (1966)].
- [6] Z. S. Gribnikov and É. I. Rashba, Characteristics of electric pinch effect in many-valley bipolar semiconductors, *Sov. Phys.–Solid State* **9**, 760 (1967) [*Fiz. Tverd. Tela* **9**, 967 (1967)].
- [7] Yu. I. Gorkun and É. I. Rashba, Electrical conductivity of crystal plates with a many-valley energy spectrum of carriers, *Sov. Phys.–Solid State* **10**, 85 (1968) [*Fiz. Tverd. Tela* **10**, 3053 (1968)].
- [8] S. I. Anisimov, V. I. Melnikov, and É. I. Rashba, Concerning one model in the theory of the Gunn effect, *JETP Lett.* **7**, 196 (1968) [*Pis'ma Zh. Eksp. Teor. Fiz.* **7**, 253 (1968)].
- [9] V. Ya. Kravchenko and É. I. Rashba, Theory of the classical size effect in the electric conductivity of semimetals, *Sov. Phys.–JETP* **29**, 918 (1969) [*Zh. Eksp. Teor. Fiz.* **56**, 1713 (1969)].
- [10] É. I. Rashba, Z. S. Gribnikov, and V. Ya. Kravchenko, Anisotropic size effects in semiconductors and semimetals, *Sov. Phys.–Usp.* **19**, 361 (1976) [*Usp. Fiz. Nauk* **119**, 3 (1976)].
- [11] V. A. Kochelap, V. N. Sokolov, and K. W. Kim, Domains of electrically induced valley polarization in two-dimensional Dirac semiconductors, *Phys. Rev. B* **104**, 075403 (2021).
- [12] A. Rycerz, J. Tworzydło, and C. W. J. Beenakker, Valley filter and valley valve in graphene, *Nat. Phys.* **3**, 172 (2007).
- [13] J. R. Schaibley, H. Yu, G. Clark, P. Rivera, J. S. Ross, K. L. Seyler, W. Yao, and X. Xu, Valleytronics in 2D materials, *Nat. Rev. Mater.* **1**, 16055 (2016).
- [14] W. Yao, D. Xiao, and Q. Niu, Valley-dependent optoelectronics from inversion symmetry breaking, *Phys. Rev. B* **77**, 235406 (2008).
- [15] I. Žutić, J. Fabian, and S. Das Sarma, Spintronics: Fundamentals and applications, *Rev. Mod. Phys.* **76**, 323 (2004); J. Sinova, S. O. Valenzuela, J. Wunderlich, C. H. Back, and T. Lügner, Spin Hall effects, *ibid.* **87**, 1213 (2015).
- [16] R. A. Moffatt, B. Cabrera, B. M. Corcoran, J. M. Kreikebaum, P. Redl, B. Shank, J. J. Yen, B. A. Young, P. L. Brink, M. Cherry, A. Tomada, A. Phipps, B. Sadoulet, and K. M. Sundqvist, Imaging the oblique propagation of electrons in germanium crystals at low temperature and low electric field, *Appl. Phys. Lett.* **108**, 022104 (2016).
- [17] C. E. Nebel, Electrons dance in diamond, *Nat. Mater.* **12**, 690 (2013); J. Isberg, M. Gabrysch, J. Hammersberg, S. Majidi, K. K. Kovi, and D. J. Twitchen, Generation, transport and detection of valley-polarized electrons in diamond, *ibid.* **12**, 760 (2013).
- [18] S. A. Parameswaran and V. Oganessian, Unfinished bismuth, *Nat. Phys.* **8**, 7 (2012); Z. Zhu, A. Collaudin, B. Fauqué, W. Kang, and K. Behnia, Field-induced polarization of Dirac valleys in bismuth, *ibid.* **8**, 89 (2012).
- [19] O. Gunawan, Y. P. Shkolnikov, K. Vakili, T. Gokmen, E. P. De Poortere, and M. Shayegan, Valley Susceptibility of an Interacting Two-Dimensional Electron System, *Phys. Rev. Lett.* **97**, 186404 (2006).
- [20] O. Gunawan, B. Habib, K. Vakili, E. P. De Poortere, and M. Shayegan, Quantized conductance in an AIAs two-dimensional electron system point contact, *Phys. Rev. B* **74**, 155436 (2006).
- [21] M. Shayegan, E. P. De Poortere, O. Gunawan, Y. P. Shkolnikov, E. Tatum, and K. Vakili, Two-dimensional electrons occupying multiple valleys in AIAs, *Phys. Status Solidi B* **243**, 3629 (2006).
- [22] K. Eng, R. N. McFarland, and B. E. Kane, Integer Quantum Hall Effect on a Six-Valley Hydrogen-Passivated Silicon (111) Surface, *Phys. Rev. Lett.* **99**, 016801 (2007).
- [23] R. N. McFarland, T. M. Kott, L. Sun, K. Eng, and B. E. Kane, Temperature-dependent transport in a sixfold degenerate two-dimensional electron system on a H-Si(111) surface, *Phys. Rev. B* **80**, 161310(R) (2009).
- [24] T. M. Kott, B. Hu, S. H. Brown, and B. E. Kane, Valley-degenerate two-dimensional electrons in the lowest Landau level, *Phys. Rev. B* **89**, 041107(R) (2014).
- [25] A. Gold, Theory of transport properties of the sixfold-degenerate two-dimensional electron gas at the H-Si(111) surface, *Phys. Rev. B* **82**, 195329 (2010).
- [26] T. Ando, A. B. Fowler, and F. Stern, Electronic properties of two-dimensional systems, *Rev. Mod. Phys.* **54**, 437 (1982).
- [27] F. Amet and G. Finkelstein, Could use a break, *Nat. Phys.* **11**, 989 (2015); Y. Shimazaki, M. Yamamoto, I. V. Borzenets, K. Watanabe, T. Taniguchi, and S. Tarucha, Generation and detection of pure valley current by electrically induced Berry curvature in bilayer graphene, *ibid.* **11**, 1032 (2015); M. Sui, G. Chen, L. Ma, W.-Y. Shan, D. Tian, K. Watanabe, T. Taniguchi, X. Jin, W. Yao, D. Xiao, and Y. Zhang, Gate-tunable topological valley transport in bilayer graphene, *ibid.* **11**, 1027 (2015).
- [28] R. V. Gorbachev, J. C. W. Song, G. L. Yu, A. V. Kretinin, F. Withers, Y. Cao, A. Mishchenko, L. V. Grigorieva, K. S. Novoselov, L. S. Levitov, and A. K. Geim, Detecting topological currents in graphene superlattices, *Science* **346**, 448 (2014).
- [29] J. Lee, K. F. Mak, and J. Shan, Electrical control of the valley Hall effect in bilayer MoS<sub>2</sub> transistors, *Nat. Nanotechnol.* **11**, 421 (2016).
- [30] K. F. Mak, K. L. McGill, J. Park, and P. L. McEuen, The valley Hall effect in MoS<sub>2</sub> transistors, *Science* **344**, 1489 (2014).
- [31] D. Xiao, G.-B. Liu, W. Feng, X. Xu, and W. Yao, Coupled spin and valley physics in monolayers of MoS<sub>2</sub> and other group-VI dichalcogenides, *Phys. Rev. Lett.* **108**, 196802 (2012).
- [32] S. Wu, J. S. Ross, G.-B. Liu, G. Aivazian, A. Jones, Z. Fei, W. Zhu, D. Xiao, W. Yao, D. Cobden, and X. Xu, Electrical tuning of valley magnetic moment through symmetry control in bilayer MoS<sub>2</sub>, *Nat. Phys.* **9**, 149 (2013).
- [33] Y. Kim and J. D. Lee, Anomalous electron dynamics induced through the valley magnetic domain: A pathway to valleytronic current processing, *Nano Lett.* **19**, 4166 (2019).
- [34] J. Jeon, Y. Kim, and J. D. Lee, Electrical Control of the Valley Magnetic Domain and Anomalous Electron Trans-

- port in Bilayer MoS<sub>2</sub>, *Phys. Rev. Appl.* **15**, 024020 (2021).
- [35] E. H. Hwang and S. Das Sarma, Valley-dependent two-dimensional transport in (100), (110), and (111) Si inversion layers at low temperatures and carrier densities, *Phys. Rev. B* **87**, 075306 (2013); Transport properties of two-dimensional electron systems on silicon (111) surfaces, *Phys. Rev. B* **75**, 073301 (2007).
- [36] V. A. Kochelap, V. I. Pipa, V. N. Piskovoi, and V. N. Sokolov, Theory of many-valued equilibrium distribution of carriers in many-valley semiconductors, *Sov. Phys. JETP* **34**, 1340 (1972) [*Zh. Eksp. Teor. Fiz.* **61**, 2504 (1971)].
- [37] V. A. Kochelap and V. N. Sokolov, Phase transition in multi-valley semiconductors in a magnetic field, *Sov. Phys. JETP* **38**, 408 (1974) [*Zh. Eksp. Teor. Fiz.* **65**, 823 (1973)].
- [38] W. L. Bloss, L. J. Sham, and V. Vinter, Interaction-Induced Transition at Low Densities in Silicon Inversion Layer, *Phys. Rev. Lett.* **43**, 1529 (1979).
- [39] J. Li, M. Gorica, N. P. Wilson, A. V. Stier, X. Xu, and S. A. Crooker, Spontaneous Valley Polarization of Interacting Carriers in a Monolayer Semiconductor, *Phys. Rev. Lett.* **125**, 147602 (2020).
- [40] Md. S. Hossain, M. K. Ma, K. A. Villegas-Rosales, Y. J. Chung, L. N. Pfeiffer, K. W. West, K. W. Baldwin, and M. Shayegan, Spontaneous Valley Polarization of Itinerant Electrons, *Phys. Rev. Lett.* **127**, 116601 (2021).
- [41] Z. S. Gribnikov, V. A. Kochelap, and V. V. Mitin, Multivalued Sasaki effect in many-valley semiconductors, *Sov. Phys. JETP* **32**, 991 (1971) [*Zh. Eksp. Teor. Fiz.* **59**, 1828 (1970)].
- [42] M. Asche, H. Kostial, and O. G. Sarbey, Experimental proof of the multivalued Sasaki effect in n-Si, *J. Phys. C: Solid State Phys.* **13**, L645 (1980).
- [43] P. N. Butcher, The Gunn effect, *Rep. Prog. Phys.* **30**, 97 (1967).
- [44] Y. Jiang, T. Low, K. Chang, M. I. Katsnelson, and F. Guinea, Generation of Pure Bulk Valley Current in Graphene, *Phys. Rev. Lett.* **110**, 046601 (2013).
- [45] R. Carrillo-Bastos, C. León, D. Faria, A. Latgé, E. Y. Andrei, and N. Sandler, Strained fold-assisted transport in graphene systems, *Phys. Rev. B* **94**, 125422 (2016).
- [46] É. Lantagne-Hurtubise, X.-X. Zhang, and M. Franz, Dispersive Landau levels and valley currents in strained graphene nanoribbons, *Phys. Rev. B* **101**, 085423 (2020).
- [47] I. S. Gradshteyn and I. M. Ryzhik, *Table of Integrals, Series, and Products*, 7th ed., edited by A. Jeffery and D. Zwillinger (Academic, New York, 2007), p. 126.
- [48] W. Melitz, J. Shen, A. C. Kimmel, and S. Lee, Kelvin probe force microscopy and its application, *Surf. Sci. Rep.* **66**, 1 (2011).
- [49] O. Kazakova, R. Puttock, C. Barton, H. Corte-Leon, M. Jaafar, V. Neu, and A. Asenjo, Frontiers of magnetic force microscopy, *J. Appl. Phys.* **125**, 060901 (2019).
- [50] O. D. Kellogg, *Foundations of Potential Theory* (Springer, Berlin, 1967), Chap. 6, p. 172.
- [51] G. A. Korn and T. M. Korn, *Mathematical Handbook for Scientists and Engineers: Definitions, Theorems, and Formulas for Reference and Review* (McGraw-Hill, New York, 1968), Chap. 15, p. 515.
- [52] A. D. Polyaniin and A. V. Monzhirev, *Handbook of Integral Equations* (Chapman and Hall/CRC Press, Boca Raton, FL, 2008, 2nd ed.), Chap. 14, p. 707.